A Theory of Local and Global Processes Which Affect Solar Wind Electrons 2. Experimental Support

JACK D. SCUDDER

NASA/Goddard Space Flight Center, Laboratory for Extraterrestrial Physics Greenbelt, Maryland 20771

STANISLAW OLBERT

Department of Physics and Center for Space Research, Massachusetts Institute of Technology Cambridge, Massachusetts 02139

We have extended the theoretical considerations of Scudder and Olbert (1979) (hereafter called paper 1) to show from the microscopic characteristics of the Coulomb cross section that there are three natural subpopulations for plasma electrons: the subthermals with local kinetic energy $E < kT_c$, the transthermals with $kT_c < E < 7kT_c$, and the extrathermals $E > 7kT_c$. We present experimental support from three experimental groups on three different spacecraft over a radial range in the interplanetary medium for the five interrelations projected in paper 1 between solar wind electron properties and changes in the interplanetary medium: (1) subthermals respond primarily to local changes (compressions and rarefactions) in stream dynamics; (2) the extrathermal fraction of the ambient electron density should be anticorrelated with the asymptotic bulk speed; (3) the extrathermal 'temperature' should be anticorrelated with the local wind speed at 1 AU; (4) the heat flux carried by electrons should be anticorrelated with the local bulk speed; and (5) the extrathermal differential 'temperature' should be nearly independent of radius within 1 AU. From first principles and the spatial inhomogeneity of the plasma we show that the velocity dependence of Coulomb collisions in the solar wind plasma produces a bifurcation in the solar wind electron distribution function at a transition energy E*. This energy is theoretically shown to scale with the local thermal (that is, approximately the core) temperature as $E^*(r) \simeq 7kT_c(r)$. This scaling is observationally supported over the radial range from 0.45 to 0.9 AU by Mariner 10 data and Imp data acquired at 1 AU. The extrathermals, defined on the basis of Coulomb collisions, are synonymous with the subpopulation previously labeled in the literature as the 'halo' or 'hot' component. If the transition energy should be required to equal the polarization potential energy $e\Phi(r)$ for all radii beyond the observer, (as motivated by Mariner 10 data) the thermal electrons should obey a polytrope law with index $\gamma = 7/6$. In this circumstance the polarization potential is equal to the specific enthalpy: $e\Phi(r) = [\gamma/(\gamma - 1)]kT_c(r)$. This relation probably does not obtain in the corona, inside $r < 10$–$20R_S$ (cf. paper 1). In the asymptotic spherically symmetric solar wind the inverse power law index for radial variation required for the thermal electrons should be $\alpha = 1/3$, which is consistent with the recent in situ determinations between 0.45 and ~3 AU. We thus provide the first self-consistent argument for associating $E^*(r)$ with $e\Phi(r)$. This theoretical asymptotic ($r \to \infty$) thermal electron temperature variation is between the conduction dominated (2/7) and the inviscid solution (2/5). In the proximity of the ecliptic the ratio of the thermal electron Coulomb mean free path to scale length is shown to decrease with increasing radial distance. By contrast, over the solar poles the same asymptotic temperature and density variations imply that the Coulomb thermal mean free path will increase with increasing radial distance. A straightforward extension of our model to slow time dependent situations shows that the fundamental scaling of E^* with temperature and, by inference, the polytrope law for thermal electrons is theoretically maintained within compression and rarefaction regions. An illustrative calculation is given of the extrathermal density's response in stream compressions near 1 AU. These calculations show that the extrathermal electron density can either increase or decrease depending on whether the core electrons compress more nearly as an isothermal gas or an adiabatic one. On the basis of these calculations and a reexamination of published data we suggest that the extrathermal density is probably enhanced within stream compression regions. This implies (as observed) that (1) the core electrons should compress more nearly as an isothermal ($\gamma \simeq 1$) rather than as an adiabatic ($\gamma \simeq 5/3$) gas and (2) a very large electron heat flux should be observed leaving the compression region along the magnetic field. We thus conclude that the global and local Coulomb effects discussed in paper 1 and elaborated here are essential aspects of the solar wind plasma as it is observed. The experimental support which the predictions of the theory in paper 1 enjoy strongly suggests that the further development of that theory is warranted with the ultimate objective of understanding the impact that global heat transport has on the physics of coronal expansions.

1. INTRODUCTION

There is, even now, no self-consistent theoretical understanding of how the thermal and/or mechanical (wave) energy of the lower corona supports the spectrum of solar wind states observed in the interplanetary medium. The usual theoretical simplifications for wave propagation (WKB) and heat conduction (small ratio K of the mean free path to the scale height known as the Knudsen number) cannot be defended at crucial phases of the acceleration of the incipient wind.

To our knowledge there exists no fully self-consistent theory for heat transport in a Knudsen regime ($K \simeq 1$) plasma such as is found immediately above coronal holes from which the (high speed?) solar wind is thought to emanate. Various ad hoc localized collisional models have been proposed [cf. *Rawls et al.*, 1975] to allow generalizations (for $K \simeq 1$) of the local

Paper number 9A0972.
0148-0227/79/009A-0972$01 00

Spitzer [1962]–*Braginskii* [1975] result $Q = -\kappa\nabla T$, often used in solar wind models, which only rigorously applies for $K \ll 1$ in nearly homogeneous systems. We have recently suggested (*Scudder and Olbert* [1979], hereafter called paper 1) that the transport physics for solar wind electrons (which carry most of the heat flow) in the Knudsen regime should have a global character alien to these localized models; this new theory has suggested several interrelationships between experimental electron parameters in an inhomogeneous, fully ionized Knudsen regime plasma that should be implicit in solar wind electron data.

The considerable additional effort required to make this theory mathematically self-consistent (to allow accurate theoretical models of thermally driven coronal winds) is unwarranted unless these interrelationships and other predictions of the theory are supported by the ever growing data base of solar wind electron measurements. This comparison represents an extensive test of the theory, since these observations now span the radial domain of 0.3–5 AU and represent more than a decade of monitoring at the orbit of earth. If, however, the theory in its present form predicts more than it assumes, further development of this novel global theory of Knudsen regime heat transport would appear fruitful.

This paper develops the predictions of the theory and compares them with the relevant solar wind electron observables. It represents a review of the salient solar wind electron morphology as organized by the theoretical ideas of paper 1. Our objective is to evaluate the merit of that approach to the transport physics of plasma electrons in the Knudsen regime. Our conclusion is that the theory, although lacking rigor, predicts and organizes a large number of reported electron observations; by virtue of this extensive experimental support the theory warrants further development.

In the first section of this paper we develop from first principles the idea of subthermal ($E < kT_c$), thermal ($E = kT_c$), transthermal ($1 < E/kT_c < 7$), and extrathermal ($E > 7kT_c \equiv E^*$) electrons as determined by the dynamics of Coulomb collisions (k is Boltzmann's constant, and T_c is the temperature). The preceding definitions are based on the assumption that the subthermal electrons are Maxwellian. Statistical arguments identify the subthermal electrons, $E < kT_c$, as the electron subpopulation that has a greater than three-sigma chance of having a Coulomb 90° cumulative scattering while traversing a (rms) thermal speed particle's free path. This subthermal portion of f_e contains the dominant fraction of the so-called 'core' density. The transthermal subclass $kT_c < E < 7kT_c$ does not have a clear local or global character. This energy regime is statistically more local at kT_c and most global toward $7kT_c$. We demonstrate that the extrathermal subclass of electrons are those locally observed electrons which as a class have a greater than 95% chance of having had their last Coulomb collision more than one (rms) thermal electron's free path away from the observer. With experimental data taken at a variety of radial distances within and at 1 AU, we show that the breakpoint, or 'transition' energy, E^*, in the solar wind electron distribution function scales as $E^*(r) \simeq 7kT_c(r)$. This scaling is that expected for the theoretical lower bound of the Coulomb-defined extrathermal population. We thus identify the theoretical Coulomb extrathermal population with the previously described 'halo' or 'hot' component [*Feldman et al.*, 1975] and illustrate those aspects of Coulomb collisions which allow this subpopulation to be discernible in the solar wind electron velocity distribution function. In section 3 we discuss the relation of this transition energy E^* to the magnitude of the electrostatic polarization potential and develop the evidence for the polytrope behavior of thermal electrons with polytrope index $\gamma \simeq 7/6$.

These theoretical considerations of the properties of Coulomb collisions in a plasma which allow the 'halo-core' dichotomy permit more precise statements of the expected correlations in steady state made in paper 1 which are developed in section 4. For the convenience of the reader we restate them here:

1. In contrast with extrathermal electrons, subthermal solar wind electrons should behave most nearly as a 'classical gas.' We define a classical gas as an ordinary gas with finite mean free path (mfp) effects (e.g., heat conduction) in contradistinction to an ideal gas where mfp = 0 (and conduction vanishes). A classical gas will compressively heat and expansively cool to the extent that heat transport allows.
2. The solar wind extrathermal fraction of the electron density should be anticorrelated with the local bulk speed (if it is nearly the asymptotic wind speed).
3. The extrathermal electrons should generally form a subpopulation of the electron component of the solar wind plasma characterized by a 'differential temperature' T_{ex}, distinguishable from T_c. The former temeprature is expected to be anticorrelated with the local bulk speed at 1 AU. The ratio T_{ex}/T_c is determined by the ratio of the average collisional depths to the corona of each subpopulation.
4. The heat flux carried by electrons should be anticorrelated with bulk speed.
5. The differential temperature of extrathermals should be nearly independent of radius in the inner heliosphere ($r < 1$ AU). Section 4 contains the experimental support from new data (Mariner 10) and from those previously published (Imp, Helios) for the above stated relations.

In the final section we discuss a simple extension of our steady state model to the case of slowly evolving stream patterns, which is the general situation at stream-stream boundaries. We calculate there the response of the halo density within compression regions and illustrate its sensitivity (through the induced gradients of the core electron properties) to the local modifications of the polarization potential.

2. General Features of the Observed and Theoretical Electron Velocity Distribution Function

The solar wind electron velocity distribution function is generally observed at all radial distances to be nearly Maxwellian in shape at low energies (the so-called core) with a smooth monotonic transition to a hotter, sparser, but nearly isotropic suprathermal population (the so-called halo). To illustrate this point, four representative examples of cuts through the velocity distribution at different radial locations are displayed in Figure 1. Velocity distribution functions with these general shapes were theoretically calculated in paper 1. The generality of those shaped solutions is not obvious, given that radial profiles had to be assumed in the 'bootstrap' calculations presented there. By very general arguments we shall show in this section that such an electron velocity distribution function is almost unavoidable for a plasma locally in the Knudsen regime that is part of an inhomogeneous plasma system such as is found within the heliospheric cavity. In so doing we also indicate additional theoretical predictions of the expected scaling of the transition energy between thermal and suprathermal subpopulations. We shall contrast the theory

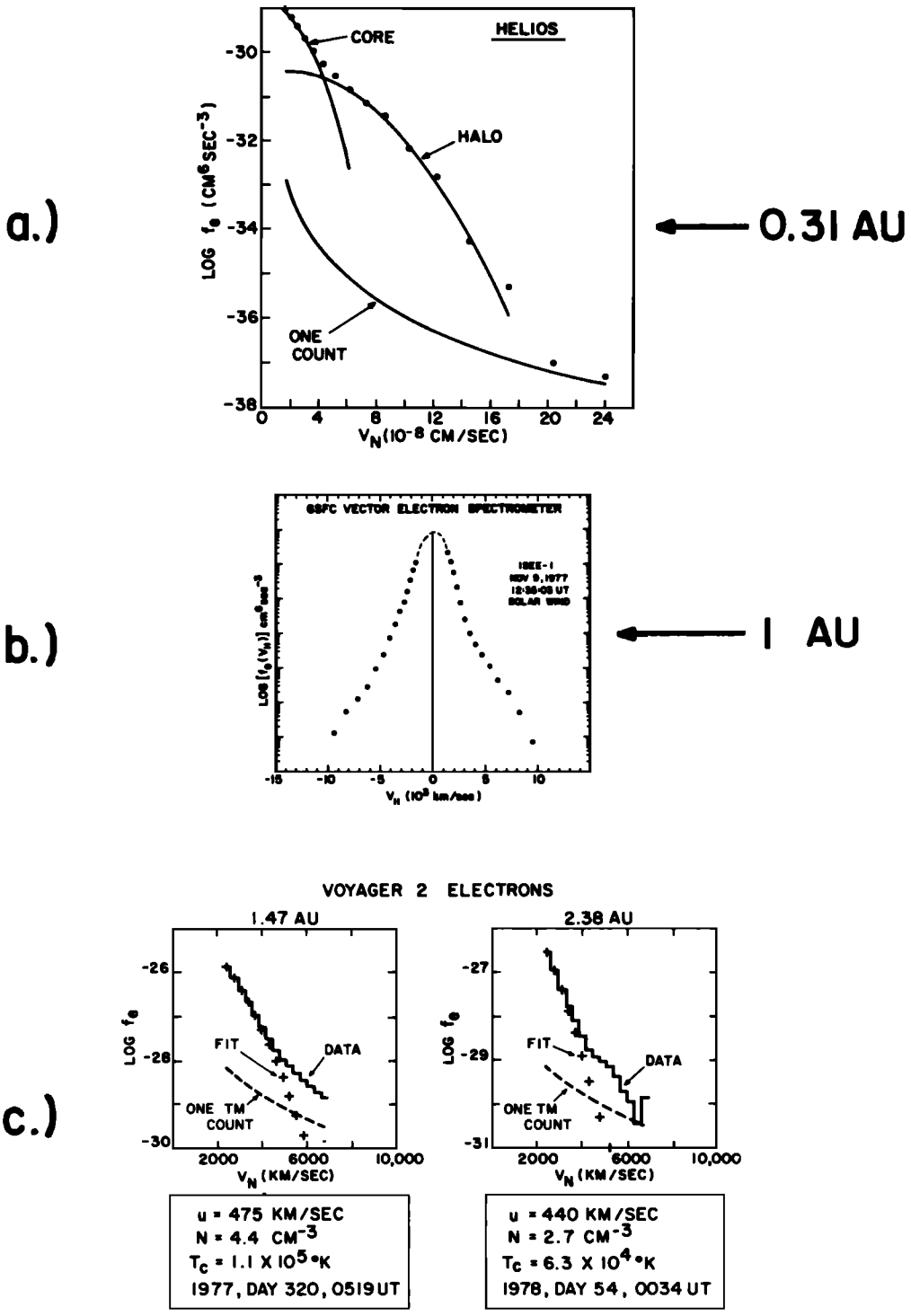

Fig. 1. Cuts of observed representative electron velocity distribution functions from Helios [*Rosenbauer et al.*, 1977], Isee 1 [*Scudder and Olbert*, 1978], and Voyager 2 [*Sittler et al.*, 1978] showing the pervasive core-halo morphology of solar wind electrons. Panels (*a*) and (*c*) show unidirectional 'slices' through $f(\hat{v})$, while the Isee 1 example (*b*) shows a full bidirectional slice through $f(\hat{v})$ along the local magnetic field direction. Example (*b*) clearly shows the skew of f, which indicates a nonnegligible heat flow.

with experimental data and show that the expected scaling is indeed observed.

We suggested in paper 1 that the extrathermal subpopulation of solar wind electrons were last members of collisional distributions much nearer to the corona than the corresponding place for the thermal electrons. Qualitatively, the situation is analogous to the situation in radiative transfer, where the same observer at different energies (frequencies) is at different collisional (optical) depths to the 'source' of the phase density (emission).

'Survival' Probabilities

The Coulomb collisional momentum transfer scattering frequency may be written as

$$\nu = \frac{\nu_{ep}\mathscr{P}(u, f_e, f_p)}{u^3\mathscr{P}(1, f_e, f_p)}$$

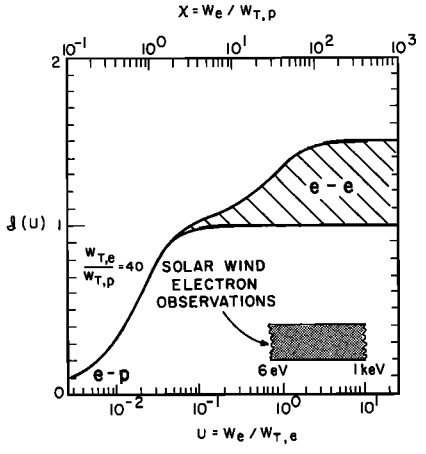

Fig. 2. Thermal spread integral of 'targets,' $\mathscr{J}(u)$, versus scaled proper frame electron speed $u = w_e/w_{T,e}$ lower horizontal axis, or $\chi = w_e/w_{T,p}$, upper horizontal axis. For the purpose of illustration we have chosen $w_{T,e}/w_{T,p} = 40$, which corresponds to $T_e \sim T_p$. For all the considerations, $T_p \ll (m_p/m_e)T_e \sim 1836T_e$, the structure of $\mathscr{J}$ is as shown.

where $u = w/w_{T,e}$ (w being the proper frame speed and $w_{T,e} = (3\ kT_e/m_e)^{1/2}$) and where the collision frequency ν_{ep} and integral $\mathscr{J}(u)$ are as defined in paper 1. The inverse cubic dependence of ν on 'test' particle proper frame speed is the well-known two-body Coulomb result. The dimensionless integral $\mathscr{J}$ accounts for the thermal motions of the electron and ion 'targets' with which a test electron interacts. The speed dependence of $\mathscr{J}(u)$ is of some interest in defining natural subpopulations of electrons with regard to Coulomb collisions. This functional dependence is illustrated in Figure 2 for Maxwellian electron and ion distribution functions of nearly equal temperatures ($T_e/T_p = 40(m_e/m_p)^{1/2} \sim 0.93$) for the range of test electron speeds much less than the ion target's (rms) thermal speed $w_{T,p}$ to speeds much larger than the electron target's (rms) thermal speed $w_{T,e}$.

There are two contributions to $\mathscr{J}(u)$: (1) that due to the test electrons' scattering off of target ions and (2) that due to test electrons' scattering off of target electrons. The hatched portion of Figure 2 indicates the electron-electron scattering contribution to $\mathscr{J}(u)$. The remaining distance below the curve results from electron-ion scattering. From this graph it is clear at a given speed anywhere on this diagram that *e-p* scattering, which is an elastic process, is the dominant contribution to $\mathscr{J}(u)$. Almost all solar wind electrons are suprathermal insofar as ion most probable speeds are concerned (i.e., $w/w_{T,p} \gg 1$), which implies that the electron-proton portion of $\mathscr{J}(u)$ is $\simeq 1$. However, as the stippled ribbon in this figure indicates, typical solar wind electron observations straddle the similar thermal to suprathermal transition of electrons scattering off of background electrons. For electrons of speeds $w \gg \simeq 2w_{T,e}$, $\mathscr{J}(u)$ asymptotically approaches 3/2. Physically, this arises from the fact that the momentum transfer is most efficient for particles of comparable speed and there are at these speeds very few additional target electrons available.

Using the probability concepts of paper 1 we desire to calculate as a function of proper frame speed the probability P_{scatter}

$$P_{\text{scatter}} = 1 - P_{\text{survival}}$$

that a test electron will be scattered while traversing a slab of thickness ΔZ equal to the local Coulomb free path $\bar{\lambda}_{\text{mfp}}$, computed for the (rms) thermal speed of the electron, $w_{T,e}$. We thus obtain

$$P_{\text{survival}}(\Delta Z = \bar{\lambda}_{\text{mfp}}, u) = \exp(-[\mathscr{J}(u)/\mathscr{J}(1)]/u^4)$$

which is plotted in Figure 3. The solid curve indicates the probability of survival (right axis) (of being scattered (left axis)) as a function of scaled proper frame speed $u = w/w_{T,e}$. The cross-hatched region indicates the typical regime of solar wind plasma electron mesaurements at 1 AU.

Test electrons with proper frame speeds greater than

$$w^* = u^* w_{T,e} \qquad u^* = 2.16 \qquad (3\sigma)$$

will transit $\bar{\lambda}_{\text{mfp}}$ unaffected by Coulomb collisions with a greater than 3σ probability. Nevertheless, there is a finite (<5%) probability of local interaction with the ambient targets. We have called this statistically defined subpopulation the 'extrathermal' electrons, since their collisional antecedents are beyond those of the thermal population.

The electrons of intervening speeds $(\frac{2}{3})^{1/2}w_{T,e} < w < u^*\ w_{T,e}$ are the 'transthermals' and have intermediate chances of scattering (survival), as may be determined from Figure 2.

Electrons with speeds $w < (\frac{2}{3})^{1/2}w_{T,e}$ have a greater than 3σ chance of being scattered while traversing one $\bar{\lambda}_{\text{mfp}}$. These particles have proper frame energies of less than kT, and we have called them the 'subthermals.'

We now address the question of how the preceding calculations allow for a bifurcation of the electron distribution function. Thermodynamic equilibrium is a situation where extrathermal electron departures and arrivals to the observer are in detailed balance; in the strict sense of the word, thermodynamic equilibrium can obtain only in a homogeneous medium. In this circumstance the shape of the distribution function is time independent even though individual extrathermal electrons are constantly moving quasi-ballistically further than the thermal electron's mean free path $\bar{\lambda}_{\text{mfp}}$ between collisions. In contrast with this 'homogeneous' thermodynamic equilibrium the solar wind processes take place in a radically inhomogeneous plasma. As is shown in Figures 5, 6, and 7 of paper 1, there are strong gradients in the density and the smooth forces implied in the solar wind expansion which affect the evolution of the distribution function even in portions of the solar cavity where gradients are weak! Most astrophysical plasmas are inhomogeneous ultimately as a result of gravitational fields; this fact plus the Coulomb 'window' above u^* permits more dense extrathermals in one proximity to 'leak' through to the local medium and show up as an overpopulated extrathermal population relative to the local collisional Maxwellian which has (by inhomogeneity) a different density and/or temperature.

Because of the properties of Coulomb collisions in a plasma and the inhomogeneous nature of the solar wind plasma, we therefore expect a noticeable change in the shape of the electron distribution function in the vicinity of the proper frame kinetic 'transition' or breakpoint energy $E_{\text{Theory}}{}^*$ defined by

$$E_{\text{Theory}}{}^* = \tfrac{3}{2}(u^*)^2 kT_c \simeq 7kT_c \qquad (1)$$

Because the preceding definition has been made on the basis of the statistical probability of Coulomb interactions, we should expect a dispersion of the experimental determination of u^*.

A transition energy $E_{\text{Data}}{}^*$ referring to the breakpoint energy may be determined directly from the data. It has been

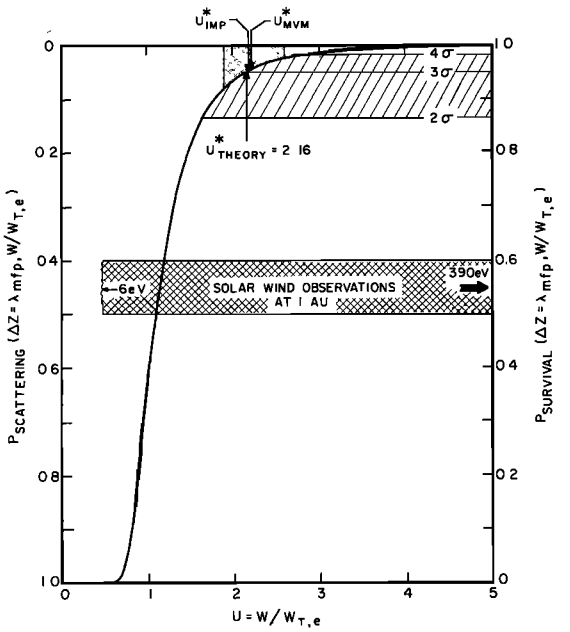

Fig. 3. Probability that a 'test' electron will survive (right axis), (scatter (left axis)) while traversing the local root mean square target electron mean free path $\bar{\lambda}_{mfp}$, as a function of scaled proper frame speed $u = w/w_{T,e}$. The theoretical 3σ definition of 'survival' is u^*_{Theory}. Other horizontal axes about this 3σ level indicate 2σ and 4σ definitions of survival. Here u_{Imp}^* (= 2.19) and u_{MVM}^* (= 2.21) are empirical determinations of the transition energy of f_e from Imp data and Mariner 10 (Mariner-Venus-Mercury, 1973) data—discussed in the text in detail. The cross-hatched zone is the entire extent of the experimental deviations from the most probable values u_{MVM}. Imp data were taken at 1 AU, and MVM data between 0.45 and 0.9 AU.

customary to fit the thermal electrons and suprathermal electrons with two separate (bi-) Maxwellian profiles. This is empirically motivated by the sharp transition of slopes of the ln f_e versus E plot between two straight segments which approximate the transthermals and extrathermal electrons, respectively, in our recent terminology.

We now offer quantitative support from in situ measurements of the transition energy of solar wind electrons.

E_{Data}^* *Mariner 10 (MVM 1973)*

We have determined the transition energy from the data acquired by the Plasma Science Experiment (PSE) on Mariner 10 between 0.45 and 0.9 AU. This breakpoint energy has been operationally determined as that proper frame energy where the core and halo Maxwellian model profiles intersect. The core and halo fits were made [cf. *Ogilvie and Scudder*, 1978] to data on either side of the break in the observed distribution function; as such, E_{Data}^* is the intersection of the extrapolated fit profiles. Nevertheless, E_{Data}^* quantifies a region of relatively strong curvature of ln f versus E, between thermal and suprathermal electrons.

In Figure 4 we illustrate, in histogram form, all of the hourly averaged scaled breakpoint energies $E_{MVM}^*(r)/kT_c(r)$, where $T_c(r)$ is the core temperature at radial distance r obtained by the Mariner 10 PSE. The functional scaling by kT_c is that suggested above by the Coulomb theory of the transition energy. The binned quantity is dimensionless, allowing data with disparate temperatures at various radial positions to be analyzed together. The binning has also been done for disjoint radial subintervals with results similar to those shown in Figure 4. We thus suggest that the superposition of observations from different radial positions gives a statistical description unbiased by radial variations. In particular, the width is what an observer should see with comparable statistics at a fixed radius. The principle features of this histogram are its modal and average values,

$$\left.\frac{E_{MVM}^*(r)}{kT_c(r)}\right|_{modal} = 7.37 \qquad \left.\frac{E_{MVM}^*(r)}{kT_c(r)}\right|_{average} = 7.87$$

its narrowness, and its extreme values,

$$5.5 \le \frac{E_{MVM}^*(r)}{kT_c(r)} \le 10.5$$

From these values we infer a spread of scaled speeds $1.91 < u^* < 2.64$ about most probable and average values of

$$u_{MVM}^*|_{modal} = 2.21 \qquad u_{MVM}^*|_{average} = 2.29$$

The above numerical relations were determined between 0.45 and 0.9 AU. The modal value has been indicated by the arrow in Figure 3. The entire range of u_{MVM}^* is given by the vertical stippled zone. This experimentally determined scaled break speed nearly equals the theoretical value (2.16) discussed above where there is a three-sigma (95%) chance of transiting the (rms) thermal electron's free path at the observer unaffected by Coulomb pitch angle effects. It is interesting to note that the experimental range of u^* for all Mariner 10 data indicated by the vertical stippled zone in Figure 3 is very nearly centered (logarithmically) within the theoretical 2σ and 4σ criteria of definition of the extrathermal subpopulation (the horizontal diagonally shaded zone in Figure 3). We interpret this break in the slope of ln f_e versus E in the vicinity of $E \simeq 7kT_c$ as the lower limit of the extrathermal component defined above.

E_{Data}^*, *Imp*

In order to show that other experimental data at another spatial location give similar results consistent with our modal and intrinsic extreme values of E_{MVM}^*/kT_c we reproduce in Figure 5 the correlation data of E_B versus T_c from *Feldman et al.* [1975]. These authors describe (p. 4192) how E_B was opera-

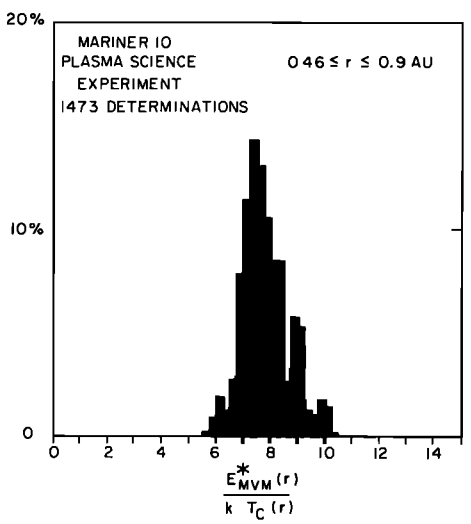

Fig. 4. Histogram of empirically determined breakpoint energy $E_{MVM}^*(r)$ from Mariner 10 Plasma Science Experiment data scaled by the local core temperature $T_c(r)$; k is Boltzmann's constant.

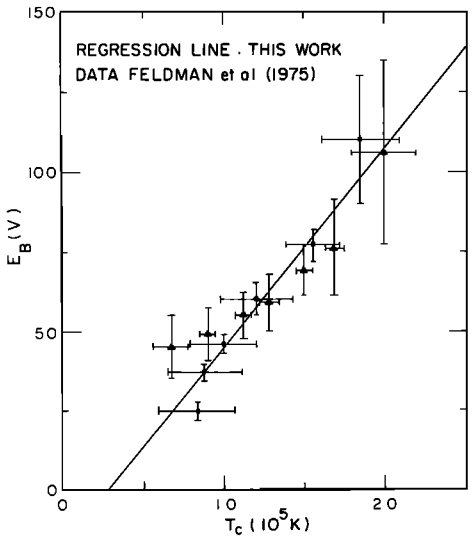

Fig. 5. Correlation profile (data from *Feldman et al.* [1975, Figure 18]) of breakpoint energy E_B defined by *Feldman et al.* [1975] and core temperature. Optimal linear hypothesis of regression assuming errors in both variables superposed from the current analysis.

tionally determined: 'The boundary between halo and core components ··· is that energy above which the count rates first exceed the count rate predicted by the best fit function f_c (fit to the lower energies) by more than 1.5 standard deviations.' E_B is the breakpoint energy (placed midway between that energy level determined above and the next [sic] lower) averaged over the four energy sweeps (covering a 90° sector) which bracket the heat flux direction $\hat{Q}_e$.' 'The error in determining E_B is about $\pm 1/4$ the energy level spacing. This is variable, since the Imp levels are logarithmically spaced, but for $E_B \sim$ 60 V, $\sigma_{EB} \simeq 5$ V.'

The best linear model of the form $E_B = A + BkT_c$ for these data has been overlaid in Figure 5. This line has the equation

$$E_B\,(\text{eV}) = -17.5\ \text{eV} + 7.25kT_c\,(\text{eV})$$

From this analysis the optimal variation of E_B versus T_c is

$$B = dE_B/d(kT_c) \simeq 7.25^{+2.95}_{-1.75}$$

with an intercept value of

$$A \simeq -17.5^{+21.5}_{-29.5}\ (\text{eV})$$

The systematic differences between E_B and E^* determined via the procedure quoted above are of three types: (1) the difference between the break definitions of *Feldman et al.* [1975] near $\hat{Q}_e$ and the breakpoint E_{BA}, which is the average of E_B over all viewing angles; (2) the quantization of the energy intervals between data points in the breakpoint energy interval; and (3) the Imp breakpoint energy, determined in the spacecraft frame rather than the proper frame. The effects of type 1 are of the order of (+3.1 ± 19) eV (compare Table 1 of *Feldman et al.* [1975] with $E_B < E_{BA}$). The effects of type 2 are of the order of one-half the average energy interval of quantization present in the graph of Figure 5—this systematic effect is ~+10 eV. At 400 km/s and $E_B^*|_{S/C} \sim 60$ eV, effect 3 is a 13% uncertainty. Thus the fit intercept values of A are consistent with zero, when systematic effects are considered. The systematic uncertainty of the intercept is 13 eV. Thus E_B^* is consistent with being strictly poroportional to T_c with no offset.

The extreme values of the Imp slope determination are consistent with those determined from the Mariner 10 PSE data. This additional determination gives

$$u_{\text{Imp}}^*|_{1AU} \sim 2.19^{+0.41}_{-0.27}$$

which is certainly consistent with the theoretical 3σ value of $2.16^{+0.64}_{-0.26}$, where the theoretical dispersion arises from the 2 and 4σ definition of E_{Theory}^* (equation (1)). The variance of the slope of the Imp data is consistent with the Mariner 10 widths' being intrinsic. Both data sets over a range of radial locations are consistent with the predicted spatial invariance of u_{Theory}^*, which is predicated on the physics of Coulomb collisions.

Thus the above results suggest that the linear relationship between E_{Data}^* and T_c is a consequence of Coulomb collisional dynamics. By contrast, *Feldman et al.* [1975, p. 4184] suggest that this relationship (1) 'may be no more than the expected kinematic relation between E_B and T_c (see Appendix A)' (where these authors show that given two Maxwellian fits to the core and halo and if T_h/T_c = const then $E_B \sim kT_c$) or (2) may arise because $e\Phi$ estimated from the electron energy equation is dominated by the enthalpy term.

3. The Transition Energy—Global and Local Conditions Reconciled

Until the calculations of paper 1 based on Coulomb collisions, it had been thought that only (collisionless) exospheric theory could predict the change in the spectral shape of the electron velocity distribution function at the energy we have called the transition energy. The 'natural' explanation of this separatrix relied on the different expected behavior of two classes of collisionless electron orbits: (1) those that are energetically bound in the electrostatic polarization potential (the core) and (2) those that are free in this potential (the halo), [cf. *Jockers,* 1970; *Schultz and Eviatar,* 1972; *Perkins,* 1973]. Because the collisionless (Vlasov) exospheric problem does not provide an unambiguous solution (for example, any function of the constants of the motion is a solution), it must be pointed out that the distribution functions selected by these authors were strongly influenced by the available experimental distribution functions. Given the theoretical and empirical discussion of the previous section including Coulomb collisions and the successful calculation of steady state distribution functions in paper 1 that closely resemble real data, it is fruitful to reopen the discussion of a transition energy which depends only on local properties (from a collisional point of view) with the transition (or breakpoint) energy which is identified in collisionless exospheric theory with the polarization potential energy. This potential depends in steady state on a global distribution of electron pressure, density, and other variables along the entire tube of force. We shall develop the necessary and sufficient conditions that these two interpretations are compatible in steady state. This matching condition requires in steady state that the thermal electrons obey a polytrope law with specified polytropic index. The polytrope 'equation of state' offers the possibility of a 'local' description for the thermal electrons. The predicted value of the polytropic index predicts more nearly isothermal than adiabatic behavior as appropriate for thermal electrons. The theory makes a definite prediction of the radial variation of thermal electrons when the density variation is known. The consequences of this matching condition are shown to be remarkably accurate by direct comparison with relevant experimental data.

From the discussion of section 2 it is unclear what theoretical relationship, if any, E_{Theory}* has to the electrostatic polarization potential Φ. Nevertheless E_{Data}*, or its relatives such as E_B, are often taken to be the polarization potential energy barrier to infinity. It has been suggested, for example, that E_B responds coherently with estimates of the polarization potential inferred from the electron energy equation when the solar wind flow is nearly steady and spherically symmetric ··· [see *Feldman et al.*, 1975].

In steady state the potential energy barrier to infinity is the work required to move an electron along any given magnetic field line to infinity:

$$e(\Phi(\infty) - \Phi(r_0)) = \int_{P(r_0)}^{\infty} Z_- e\mathbf{E} \cdot d\mathbf{r} \equiv \oint Z_- eE_{\parallel}\, dl \qquad (2a)$$

where $P(r_0)$ is the observation point and $\oint$ indicates the line integral along the appropriate **B** line. The last two integrals of (2*a*) are equal as a result of the path independence. If we ignore the additional electric field in the proper frame due to the ohmic term, propagating waves, and deviations from charge neutrality in the solar wind beyond 1 AU, we have from the generalized Ohm's law (see, for example, *Rossi and Olbert* [1970])

$$Z_- e\mathbf{E} \cong \nabla P_e / n_e \qquad (2b)$$

where P_e is the electron partial pressure, n_e the electron number density, where Z_- is -1, and $e = 4.8 \times 10^{-10}$ esu. Since the electron pressure P_e is dominated by the thermal partial pressure, we may write the potential as

$$e\Phi(r_0) = kT_c(r_0)\delta(r_0) \qquad (3a)$$

where

$$\delta(r_0) = 1 + \int_{\infty}^{r_0} \frac{T_c(r)}{T_c(r_0)} \nabla(\ln n_c) \cdot d\mathbf{r} \qquad (3b)$$

where we have assigned the zero of potential at infinity.

The theoretical polarization potential $\Phi(r_0)$ scales directly with the local temperature provided $\delta(r_0)$ is a weak function of the local temperature. If this situation obtains, then

$$\delta(r_0) = \left.\frac{d(e\Phi)}{d(kT_c)}\right|_{r_0}$$

should empirically be a constant with respect to T_c variations at a fixed radial position.

From experimental data there is strong support for this idea. By combining the information in 1-AU data given by *Feldman et al.* [1975, Figures 2 and 18] and noting that E_T in these author's notation is $e\Phi$ in ours we see that

$$\delta_{\text{experimental}}|_{1\text{AU}} = \left(\frac{dE_T}{dE_B}\right) \cdot \left(\frac{dE_B}{d(kT_c)}\right) = O(1) \cdot 7.25$$

which is apparently not a function of local temperature T_c. We have used the fact as argued by those authors that (E_T, E_B) and (E_B, kT_c) are linearly correlated. It is by no means clear that (3*b*) transparently implies that $\delta(r_0)$ is nearly independent of $T_c(r_0)$; however, this appears to be empirically substantiated—at least on a statistical basis. It is therefore clear from microscopic Coulomb properties and the mathematical structure of the polarization potential that at 1 AU in steady state, E^* and $e\Phi$ should be proportial because of their common parametric dependence on the local temperature T_c.

Mariner 10 data indicate that on average $E_{\text{Data}}^*(r)/kT_c(r)$ is independent of radius between Mercury and earth. It is therefore possible, given the evidence at 1 AU, that the Mariner 10 data imply that

$$\frac{e\Phi(r)}{kT_c(r)} = \delta(r)$$

is independent of radius (so long as the conditions outside of the observer are similar to those outside of the 1-AU observer.)

Pursuing the consequences of this hypothesis in mathematical terms, we should have $d\delta(r)/dr \simeq 0$. This condition is only satisfied if the core obeys a polytrope relation for all radii beyond that of the observer:

$$\begin{aligned} P/P_0 &= (n/n_0)^{\gamma} \qquad \gamma = \delta/(\delta - 1) \\ T_c(r)/T_c(r_0) &= (n/n_0)^{(1/(\delta-1))} \qquad r > r_0 \end{aligned} \qquad (4)$$

The polytropic index $\gamma = 7/6$ is determined by the stationary value of $\delta \simeq 7$. The entire range of observed δ from Mariner 10 is 5.5–10.5 with variability in the effective electron γ of 1.10–1.22. This range of gammas is more nearly isothermal than adiabatic. This type of electron thermal behavior has been invoked previously by *Burlaga et al.* [1971], *Hundhausen and Montgomery* [1971], and *Hundhausen* [1973]. Recent theoretical modeling of two-fluid solar wind dynamics by *Goldstein and Jokipii* [1977] and V. J. Pizzo private communication, 1978), using different polytrope indices for electrons and ions, obtain (1) better agreement with observations than a one-fluid approximation and (2) tend to favor an electron γ of approximately 1.15–1.2. This range of values contains the currently suggested value of $\gamma = 7/6 = 1.1\bar{6}$. Recently, *Feldman et al.* [1978*b*] have suggested that solar wind electrons in stream interactions behave as if they obey a polytrope relation with $\gamma = 1.45$, which is more nearly adiabatic than isothermal in character. We will discuss these dynamical observations in detail in the last section of our paper, and we suggest that their observations are consistent with nearly isothermal electron behavior.

The stationary value of δ suggested by (4) implies a temperature variation when the density profile is specified. For large distances ($n \propto r^{-2}$) the condition of (4) ($\delta = 7$) suggests that the thermal temperature varies as

$$T_c(r)/T_c(r_0) = (r/r_0)^{-1/3} \qquad r > r_0 (E^* = e\Phi)$$

with a variability of exponent 0.21–0.4, which results from the extremes of the observed δ. This range is similar to that suggested by *Montgomery et al.* [1968] based on Vela data taken at 1 AU and indirect arguments. Average radial variations of thermal electrons have recently been determined on the basis of in situ observations at different radial positions. The reported power law fits in the approximate inverse square density regime are

Mariner 10 [*Ogilvie and Scudder*, 1978]

$$0.4 < r(\text{AU}) < 0.85 \qquad T_c \propto r^{-0.3 \pm 0.08}$$

Voyager 2 [*Sittler et al.*, 1978]

$$1.36 < r(\text{AU}) < 2.25 \qquad T_c \propto r^{-0.34 \pm 0.16}$$

It is also interesting to note that this polytrope law implies

TABLE 1. Composite Empirical Density Profiles for Coronal Holes and In Situ 1-AU Electron Temperature Values

	Slow Wind (400 km/s)			Fast Wind (740 km/s)		
	1.03 R_S	10 R_S	215 R_S	1.03 R_S	10 R_S	215 R_S
n_e*	6×10^8	1.3×10^4	15.9	2×10^8	4.2×10^3	4.8
T_c	(1.7×10^6)	(6.1×10^5)	1.25×10^5†	(8.9×10^5)	(3.1×10^5)	0.99×10^5†

Intermediate computed values are shown in parentheses.
**Sittler* [1978].
†*Feldman et al.* [1975, 1976].

an upper limit for the electron temperature of the corona as can be estimated along a given streamline as

$$T_c(1.03\ R_S) \gtrsim T_c(1\ \text{AU}) \left(\frac{n_e(1.03\ R_S)}{n_e(1\ \text{AU})} \right)^{1/6} \qquad (5a)$$

The inequality arises owing to the possible variation in γ toward unity inside 10–20 R_S (cf. *Parker* [1963] for arguments). If we assume $\gamma = 7/6$ to $R = 10\ R_S$ and $\gamma = 1.1$ between 1.03 and 10 R_S, we can estimate

$$T_c(1.03\ R_S) = T_c(1\ \text{AU}) \left(\frac{n(1.03\ R_S)}{n(10\ R_S)} \right)^{0.1} \cdot \left(\frac{n(10\ R_S)}{n(215\ R_S)} \right)^{1/6} \qquad (5b)$$

Using composite empirical density profiles [*Munro and Jackson*, 1977; *Sittler and Olbert*, 1977] for coronal holes and in situ 1-AU electron temperature values given in Table 1, we obtain (via (5*b*))

$$T_e(1.03\ R_S,\ U_{SW} \sim 740) = 8.9 \times 10^5\text{°K}\ (1.8 \times 10^6\text{°K})$$

$$T_e(1.03\ R_S,\ U_{SW} \sim 400) = 1.7 \times 10^6\text{°K}\ (2.3 \times 10^6\text{°K})$$

where the value in parentheses is the upper limit via $\gamma = 7/6$ independent of radius (equation (5*a*)). The intermediate computed values in Table 1 appear in parentheses. These estimates are certainly consistent with the coronal hole electron temperatures inferred from soft X ray data by *Maxson and Vaiana* [1977] of 9×10^5°K to 3×10^6°K but favor the lower portion of this range and possibly suggest that the temperatures in the source region of the high-speed wind may be lower than those for the slower wind.

It is appropriate to discuss empirical estimates of $e\Phi$. *Feldman et al.* [1975] have determined a number of parameters which characterize 1-AU electron distribution functions and have concluded (p. 4181) that 'halo electrons with energy greater than some breakpoint energy [E_{BA}] of ~60 eV' may be unbound. Comparable estimates of Φ were obtained from the electron energy equation. This is to say that $Z_- e\Phi$ (1 AU) is approximately −60 eV. The quantity used to determine this number is highly quantized (cf. p. 4183) with the effect that E_B and its relative E_{BA} are (1) systematically lower than a continuum definition would determine them to be and (2) quantized in the proximity of 60 eV in increments of size of ~20 eV. The average thermal electron internal energy (per particle) is the average of a continuous parameter (Table 1 of the same paper) and is approximately 10.6 eV, which gives an empirical estimate of

$$\delta_{\text{Experimental}} \simeq \frac{60^{+20}_{-0}}{10.6}\ \text{eV} = 6.6 \pm 0.9$$

which is clearly consistent with the theoretical value of 7.

We thus conclude that relevant experimental estimates and theoretical arguments are consistent with the theoretical ansatz that $E_{\text{Theory}}^* \cong 7kT_c$ derived from the properties of Coulomb collisions is synonymous with the polarization potential energy with respect to infinity provided (2*b*) is a valid approximation to the generalized Ohm's law along a tube of force from the observer to infinity. This is stated algebraically by

$$E_{\text{Theory}}^*(r_0) = e\Phi \simeq 7\ kT_c(r_0) \qquad (6a)$$

Within this framework the polarization potential is the specific enthalpy,

$$e\Phi(r) = \frac{\gamma}{(\gamma - 1)} kT_c(r) \simeq 7\ kT_c(r) \qquad \gamma = 7/6 \qquad (6b)$$

4. Observational Support of Theoretically Expected Correlations: Steady State

With the content of the transition energy in steady state clarified, the arguments for correlated behavior of different subpopulations of electrons with other solar wind variables are considerably simplified. We restrict our discussion in this section to steady state conditions. It should be clear from the contents of our discussion that the term 'steady state' should not be construed as meaning only the time-independent observational data gathered during some quiet time interval in the reference frame of the spacecraft. Rather, the term implies the time independence as judged by an observer in a frame corotating with the sun (or, more precisely, the frame in which the magnetic tubes of force may be considered as stationary if averaged over the fluctuations due to the possible presence of various wave modes). Since the interplanetary medium is higly structured in heliocentric azimuth, all experimental data change in time, and only a careful, preparatory analysis can decide whether a given set of observations is steady in the sense defined above. If a data set can be declared as steady in the corotating frame and yet shows temporal variations in the spacecraft frame, a great variety of predictions can be obtained from a sequence of results of paper 1, each referring to a different tube of magnetic field lines, characterized by a different state of plasma parameters within that tube. One can infer, for example, how observed changes in the magnitude of the wind velocity should be related (correlated or anticorrelated) to the theoretically expected changes in the various quantities characterizing the electron distribution. Such predicted correlations can be compared with the observed ones. Procedures of this type offer a strong test of the validity of our model.

Correlations for Thermal Electrons

As is theoretically shown in the second section of this paper, the sub- and lower-energy transthermal electrons are in the best collisional contact with the ions and other electrons. The electrostatic quasi-neutrality condition also strongly couples the electrons and ions. It is therefore not surprising that the thermal electron density should emulate that of the ions and that the electrons should have a nearly common bulk speed

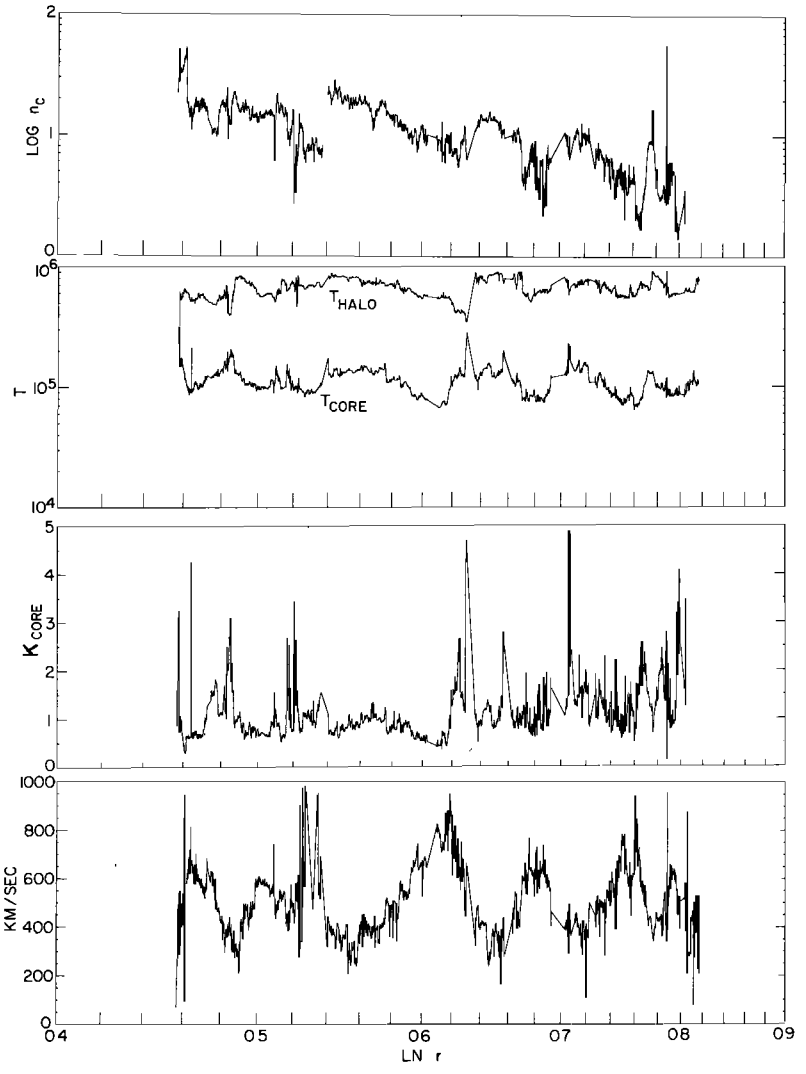

Fig. 6. Radial variation of Mariner 10 electron data. Upper panel is electron ambient density estimates. Next panel contains core and halo temperature estimate. The bottom panel is a self-consistent estimate of the plasma bulk speed from electron data from the Plasma Science Experiment.

with that of the ions. These phenomena have been reported previously starting with the work of *Montgomery et al.* [1968]. Of course, the energy exchange rate between thermal electrons and protons is still very small, so that their temperatures may be different.

Whenever the local magnetic intensity is increased as a result of pressure imbalances across a flux tube, the transverse plasma pressure will be enhanced to the extent that energy losses along B allow. In the case of ions this loss is almost negligible, and the heating proceeds essentially according to the double-adiabatic hypothesis. By contrast, even subthermal electrons have sufficient speeds to remove energy from the compression regions. This mobility is counteracted by the changes in the local polarization potential so as to maintain quasi-neutrality. These electrons nevertheless can conduct a large amount of the compressive work away from the site of the compression. This feature of electrons was discussed from a local fluid standpoint by *Hundhausen and Montgomery* [1971] and *Hundhausen* [1973]. The predicted polytrope behavior required in section 3 also allows (1) a local description of thermal electrons and (2) an equation of state that should imitate nearly isothermal behavior.

Subthermal electrons do locally Coulomb scatter off of the embedded ions and other shielding electrons which on average are moving with the local fluid velocity. Therefore if there are velocity gradient components (and therefore corresponding density and temperature variations) parallel to the local magnetic field with scale lengths comparable to or longer than the electron mean free path, a subthermal electron can gain or lose energy depending on the sign of the gradient along the particle's parallel velocity. In stream regions this effect plus thermal conduction will tend to heat (if at all) the subthermal electrons in stream compressions more isotropically than one obtains by simple adiabatic compression.

It is important to reemphasize that the work (positive or negative) done on the parallel motions of the electrons can be tapped only by those electrons which recognize the existence of scattering sites moving with different bulk speeds. In this connection the subthermal electrons have a large probability of recognizing flow gradients along B with scale lengths L of the order of the thermal free path (1/4–1/2 AU at 1 AU) which is a typical scale length along the interaction pressure ridge at overtaking streams near 1 AU (V. J. Pizzo, private communication, 1978); by way of contrast, the extrathermals have a 3σ probability of Coulomb collisionally ignoring flow gradients on such a small scale compared to their free path.

From this conclusion it appears necessary that the scale length L of bulk velocity gradients along the local tubes of force $L = U \cdot \hat{B}/\nabla(U \cdot \hat{B})$ be no shorter than $\bar{\lambda}_{mfp}$ in order that the electrons recognize the velocity gradient and compress in phase with the ions; a magnetofluid dynamic description with polytrope thermal electrons is only consistent in this circumstance. If this condition is violated (perhaps at shock boundaries where $\hat{U}$ and $\hat{B}$ are parallel throughout) then kinetic processes involving space charge and time-varying electric fields must be explicitly considered for such processes.

The radial variation of electron core temperature and electron bulk speed (among other parameters) as determined from the Mariner 10 PSE data are illustrated in Figure 6. These data span the radial range 0.45–0.85 AU. The variation of the core temperature with radius has superposed structure caused by the dynamical interaction of corotating streams. This compressive effect expected of a classical gas can be clearly seen on the leading edges of the streams shown in Figure 6. If we concentrate on the trailing edges of these streams, where dynamical effects are minimal, there is a tendency for T_c to be lower locally when U is higher. This effect is consistent with the weak inverse correlations between T_{core} and the bulk speed reported by *Serbu* [1972] and *Feldman et al.* [1975] on the basis of 1-AU observations. All of these correlations are consistent with expansive collisional cooling and compressive heating of a 'classical gas.' A complication for the former interpretation is that the electron temperatures in the coronal source regions of high-speed flows may be a priori lower than those for low-speed flows, the observations in the rarefactions being a mix of expansive cooling and initial (boundary) conditions.

Correlations for Extrathermal Electrons

The global, extrathermal component of solar wind electrons was the subject of several predictions in paper 1. We suggested there that the local bulk speed should be anticorrelated within a given corotating stream with fractional extrathermal phase density, extrathermal 'differential temperature,' and net heat flux. These correlations were not local causes and effects but were controlled by the electrical potential and the changes in collisional depth with energy of the observer relative to the distant collisional origin of the observed suprathermal phase density. The induced, local correlations given in the introduction were all consequences of the global physics of the interplanetary polarization potential and the integrated effects of the Coulomb cross section. We also suggested a theoretical reason that the halo temperature should be nearly independent of radius in the inner heliosphere. In this section we organize the experimental support for these theoretical suggestions.

In Figure 6 we also show the heliocentric variation of the halo temperature and the core Knudsen number $K_{core} = \bar{\lambda}/H$. We call attention to the strong anticorrelation of the halo differential temperature T_h with bulk speed, where

$$T_h = \left(-\frac{1}{k} \frac{[d \ln (f_e)]^{-1}}{dE} \right) \qquad E > E_{Data}^*$$

where the average $\langle\ \rangle$ is that implied by a linear least squares fit of $\ln f_e$ versus E for $E > E^*$ in the proper frame.

When the self-consistently determined bulk speed is locally high, T_h is generally low, and when the speed is lower, T_h is generally larger. The principal isolated exceptions, such as those at 0.634 and 0.485 AU, are signals of stream interfaces, discussed by *Ogilvie and Scudder* [1978], and can easily be screened out on the basis of T_c and T_h being locally anticorrelated and the large local core Knudsen number. Because of the radial variations superposed in Figure 6, it is best to rephrase our expectation that (within the stream)

$$\text{Sign}\left(\frac{dT_h}{dt}\right) = -\text{Sign}\left(\frac{d|U|}{dt}\right)$$

in order that there be no confusion. There are at least three ways to understand T_h being smaller in high- relative to low-speed solar wind: (1) perhaps there exists an omnipresent scattering agent, such as magnetic irregularities embedded in the accelerating flow; the suprathermals give up more energy (are 'cooled') in scattering off these irregularities in flows with larger spatial speed gradients (asymptotic bulk speeds higher, cf., for example, *Parker* [1963, Figure 6.1]); or (2) extrathermal electrons at 1 AU in high-speed flows have been most recently in collisional quasi-equilibrium with cooler coronal plasma than is the case in low-speed flows (the site of collisional quasi-equilibrium of the 1-AU extrathermals near the corona may be (*a*) at different solar altitudes with the underlying temperature and density profiles the same in different speed regimes as discussed in paper 1 or (*b*) at the same coronal level with the electron temperature profile different (cooler) on high-speed flux tubes than low ones); or (3) suprathermal electrons are expansively 'cooled' by global Coulomb scattering at distances separated by sufficient radial distance that the local bulk speeds at the extremes of the Coulomb suprathermal mean free path are different; in this case the suprathermals give up energy to the flow via the embedded Coulomb scatterers.

From the measurements of whistler turbulence [*Neubauer et al.*, 1977; F. M. Neubauer, private communication, 1978] it is unlikely that there exists enough appropriate turbulence to locally 'Fermi' cool the extrathermal electrons in the case of alternative 1 above. The calculations of paper 1 show that alternative 2*a* is given quantitative support, although 2*b* cannot be completely ruled out. Alternative 3 is present in either 2*a* or 2*b*. Preliminary estimates suggest that alternative 3 together with the hypothesis of coronal 'source' regions of equal temperatures for high- and low-speed winds (alternative 2*b*) do not sufficiently discriminate between flow states to provide the observed cooling. We therefore conclude that 2*a* and 3 above are consistent with theory and observations at the present time.

In Figure 6 one can also see the theoretically suggested independence of T_h (on average) with radius which has been reported previously by *Ogilvie and Scudder* [1978], who suggested a power law exponent consistent with zero.

In Figure 7 we illustrate hourly averaged Mariner 10 PSE determinations of the halo/core density fraction and the bulk speed versus heliocentric radius between 0.45 and 0.9 AU. The theoretically expected anticorrelation of the extrathermal fractional density with local bulk speed is clearly shown. These data indicate that the halo energy regime is depopulated in relation to the core in high-speed flows when compared to low-speed flows. We understand this as resulting from the higher potential energy barrier which the extrathermals must overcome in the high-speed flow relative to the low-speed flows. Since a strong, pervasive high-frequency ($\omega < \omega_{ce}$ whistler branch) turbulence field necessary to efficiently scatter halo electrons has not been directly observed in the so

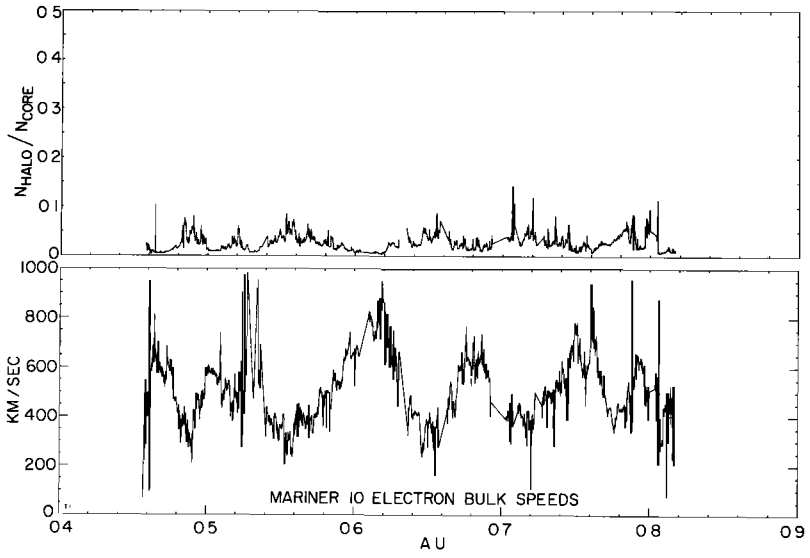

Fig. 7. (Upper panel) Variations of N_{halo}^*/N_{core}^*, where asterisk denotes ambient estimates after spacecraft potential effects have been corrected. (Lower panel) Bulk speed variations from Mariner 10 Plasma Science Experiment electron observations.

lar wind (although surveys have been made [e.g., *Neubauer et al.*, 1977] and since the effects discussed in paper 1 are unavoidable, it seems the explanation (2*a*, *b* above) of the extrathermal 'cooling' and 'depopulation' given in that paper is currently to be preferred.

We consider in Figure 8 a superposed epoch analysis of electron properties through some 'simple' very high speed streams observed at 1 AU as reported by *Feldman et al.* [1978*a*]. These independent data also show the anticorrelation of T_h with the bulk speed. Of all the quantities plotted in this figure the halo fraction of the total density n_h/n is the most volatile. We encourage the reader to inspect this record to deduce the trend he perceives in this record for the stream behind the stream maximum. We have suggested by the solid line the trend we perceive in this data. The trend is certainly not positively correlated with the bulk speed. We suggest that this data also indicate an anticorrelation with speed with the halo fraction more populous in the lower-speed region $U \sim 400$ than in the higher-speed region. This is the same sense and magnitude of the (anti-) correlation inferred from the Mariner 10 data.

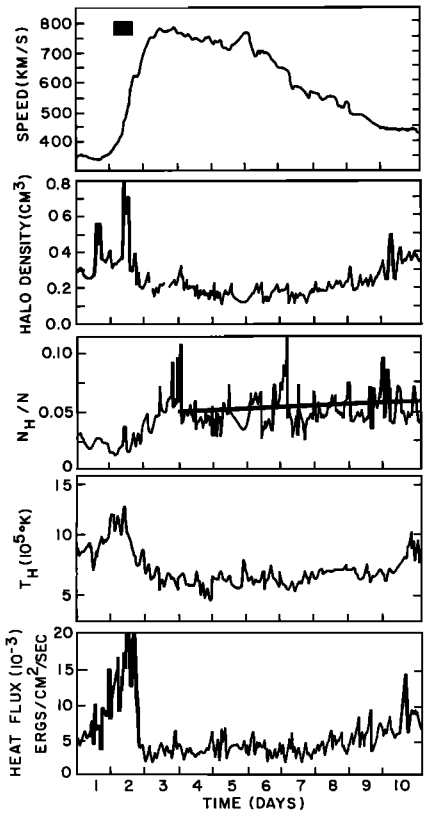

Fig. 8. Composite synthesis from *Feldman et al.* [1978*b*, Figures 6, 7, and 8], showing superposed epoch variations of selected electron parameters near a corotating stream interaction region. Black bar in speed panel denotes proton temperature enhancement.

In the bottom panel of Figure 8 we call attention to the support these data provide for the expectation that the local heat flux should be inversely related to the speed. The statistical study of *Feldman et al.* [1976] at 1 AU support the generality of this situation. In this same connection *Rosenbauer et al.* [1977] also report that the heat flux is lower on average in high-speed flows than in low-speed flows at all radial distances sampled by the Helios spacecraft ($0.3 < R$ (AU) < 1).

We thus conclude that the observational data from three independent experimental groups on three different satellites which are relevant to our steady state calculations do provide strong support for the theoretical predictions made by us in paper 1.

5. Observational Support of Theoretically Expected Correlations: Dynamics

Many of the changes seen in interplanetary electrons by an observer at a fixed radial distance are associated with stream-stream interaction pressure ridges which are not necessarily corotating or therefore 'steady' in the sense of the discussion of the previous section. We shall show in this section that the steady state theory developed in paper 1, which has been extended and supported in the previous sections, should apply within dynamical stream interaction fronts. As an example of the theory's utility and self-consistency, we shall illustrate, by direct calculation, the behavior expected of the extrathermal

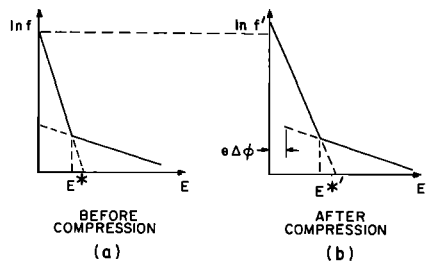

Fig. 9. Schematic of electron distribution function response to a polytropic compression of the core electrons: (*a*) unperturbed and (*b*) within compression.

phase density at compressions associated with stream-stream interactions. The theory suggests that (1) the transition energy E^*/kT_c is insensitive to dynamics and (2) the extrathermal density variation at a proton compression depends sensitively on the polytrope index γ, appropriate for thermal electrons. The observations of the halo density variation at these ridges imply that γ should have a value more nearly appropriate for isothermal ($\simeq 1$) as opposed to adiabatic (5/3) behavior. On the basis of such successful application of the theory in dynamical situations it is suggested that the theory for thermal solar wind electrons in the steady state contains the essential aspects of electron behavior even in the presence of relatively slow time variations represented by hydrodynamic disturbances.

Superimposed upon the global steady state of the interplanetary medium (in the corotating frame) there exists some intrinsic evolution of the stream patterns, for example, in response to boundary condition changes at the sun. The evolutionary readjustment of flow lines will result in temporal compressions and rarefactions of the steady state arrangement of material. Such 'waves' will propagate with a speed less than or comparable to the speed of the wind, U; the scale length of the stream-stream interaction fronts along B are typically $L \sim$ 1/4–1/2 AU at 1 AU (V. J. Pizzo, private communication, 1978). The intrinsic time scale τ of the variations experienced by the ambient plasma is of the order of L/U. This time scale is long in comparison with the transit time of most electrons through the disturbance; in other words such transient changes are slow as far as electrons are concerned, and the conclusions drawn in paper 1 from steady state considerations still apply in a semiquantitative sense. Comparison of theory with observations of such transients may therefore be of further heuristic value. With the generalizations just made, almost any stream interaction is suitable for comparison with the results to be calculated below—whether it is truly corotational or evolutionary. To illustrate this approach, we address the problem of the response of the extrathermal density and transition energy E^* at stream-stream interaction regions.

Our approach is to note that within compression (rarefaction) regions which have typical scale lengths along $\hat{B}$ larger than the local thermal electron mean free path the subthermal (or core electrons) will behave as a classical gas—they will heat (cool) in phase with the increase (decrease) of ambient density to the extent consonant with energy transport. We have previously shown by steady state considerations that thermal electrons obey a polytropic law with a $\gamma \simeq 7/6$. We will specify the polytropic form but have γ determined from experimental considerations, $P/P_0 = (n_e/n_0)^\gamma$, where P_0 and n_0 are unperturbed reference values of P and n_e, respectively, and the effective γ is somewhere between the isothermal value of 1 and the adiabatic value of 5/3.

At the same time, we note that from a collisional point of view the halo electrons have a high probability of not collisionally recognizing the change in the density of thermal electron and ion scattering centers within a compression zone of scale length $L \simeq \bar{\lambda}_{mfp}$ along the local tube of force. These particles will respond, however, to the perturbation in the polarization potential caused by the compression of the thermal electrons. The local change in the polarization potential energy of an electron relative to the ambient value at a nearby point R outside of the compression is (by generalized Ohm's law in the spirit of approximations made in deriving (2*b*))

$$e\Delta\Phi \equiv e(\Phi(r) - \phi(R)) = kT_0 \ln\left(\frac{n(r)}{n_0}\right) \qquad \gamma = 1$$

$$e\Delta\Phi \equiv e(\Phi(r) - \phi(R)) = \frac{\gamma}{\gamma - 1} k\,[T_c'(r) - T_0] \qquad \gamma \neq 1 \tag{6c}$$

where $n(r) = n_0(R) + \delta n(r)$ and $T_c'(r) = T_0(R) + \delta T(r)$; n_0 and T_0 are assumed to be the spatially independent, nearby, unperturbed values outside of the compression along the given tube of force. R denotes a place along the local tube of force removed from the compression but in the immediate vicinity of it.

We thus see that in a compression zone the polarization potential is larger than it is outside of the compression. This corresponds to a slight excess of positive charge in the zone. This additional attractive force accelerates the halo particles (which by the results of section 1 are to within 3σ) unimpeded by collisions to be observed at the kinetic energy $E(r) = E_{old}(R) + e[\Phi(r) - \Phi(R)]$ in the compressed region if they were at energy $E_{old}(R)$ outside of the compression region.

We have schematically illustrated the electron distribution function prior to encountering a compression region in Figure 9*a* and within the compression region in Figure 9*b*. A Maxwellian in this format of $\ln f_e$ versus E is a straight line. The differential temperature is proportional to the negative reciprocal of the slope of a straight line on this semilogarithmic plot. The transition energy E^* is operationally defined as the local proper frame kinetic energy where the core and halo Maxwellian parameterizations intersect. In general, $E^*(r)$ will change in a systematic manner through the compression zone under the combined responses of the core's polytropic compression and the polarization potential changes that the halo experience.

Since the halo 'density' is equal to a partial moment of the distribution function,

$$n_h = \int_{4\pi} d\Omega \int_{w^*}^{\infty} f_e(w, r) w^2\, dw \tag{7}$$

where w^* is the speed determined by the transition energy, it is not clear how the halo density will vary with space (or time for the observer $\mathbf{r} = \mathbf{r}_0 + \mathbf{U}_{SW}(t - t_0)$) through the compression.

As is shown in Figure 9*a*, the natural logarithm of the electron distribution function resembles

$$\begin{aligned} (\ln f_e)_{core} &= A_c - E/(kT_0(R)) \qquad (E \leq E^*) \\ (\ln f_e)_{halo} &= A_h - E/(kT_h(R)) \qquad (E \geq E^*) \end{aligned} \tag{8}$$

outside the compression, where A_c, A_h are given by

$$A_c = \ln\,(n_c(R)/(\pi^{3/2} w_c^3))$$

$$A_h = \ln\,(n_h(R)/(\pi^{3/2} w_h^3))$$

where $1/2\ m_e w_c^2 = kT_c$ and $1/2\ m_e w_h^2 = kT_h$. From our physical arguments regarding collisions and potential effects the modeled distribution function within the compression region at r is

$$\begin{aligned}(\ln f_e')_{\text{core}} &= A_c' - E/(kT_c') \qquad (E \le E^{*\prime}) \\ (\ln f_e')_{\text{halo}} &= A_h - (E - e\Delta\Phi)/(kT_h(R)) \qquad (E \ge E^{*\prime})\end{aligned} \tag{9}$$

where we have kept the halo temperature constant, since the dynamical compression will not, by our hypothesis, modify the 'temperature' which the coronal conditions 'impress' on the flux tube threading the compression region. For the purposes of these illustrative calculations we assume that the coronal conditions impress a constant T_h in this region. (In principle the observed T_h profile across adjacent sampled stream tubes could be substituted to refine the calculation presented below.) The $e\Delta\Phi(r)$ energy shift in the halo subpopulation equation (9) models the local gain of kinetic energy which incident halo particles experience getting from R to the observer at r. The new constant A_c' in (9) is given by

$$A_c' = A_c + \ln [n_c(r)/n_0(T_0/T_c')^{3/2}]$$

where

$$T_c'/T_0 = (n_c(r)/n_0)^{\gamma-1}$$

from the assumed polytropic law for the thermal electrons.

To calculate the halo density variation through a model compression (equation (7)) we must determine $E^{*\prime}$ as a function of position along the tube of force. By solving (8) we obtain

$$E^{*\prime}(R) = \beta k T_0 \qquad T_0 \equiv T_c(R) \tag{10a}$$

where $T_0 = T_c(R)$ and

$$\beta = \frac{T_h}{T_h - T_0} \ln [n_0/n_h \cdot (T_h/T_0)^{3/2}] \tag{10b}$$

Using $T_h/T_0 = 6$, $T_h = 7 \times 10^5$°K, and $n_0/n_h = 19$ at 1 AU, we find $\beta = 6.75$. By solving (9) we obtain

$$E^{*\prime}(r) = \beta k T_c'(r)[1 + 1/\beta \ln (n/n_0] \qquad \gamma = 1$$

$$E^{*\prime}(r) \simeq \beta k T_c'(r) \left[1 + \frac{\delta T}{(T_h - T_0)} \cdot \left(1 + \frac{(5 - 3\gamma)T_h - 2\gamma T_0}{2\beta(\gamma - 1)T_0}\right)\right] \qquad \gamma \neq 1 \tag{11}$$

It is important to note that the corrections terms to unity in the above two expressions are very small at 1 AU for typical excursions of the density and temperature. Thus even in stream-stream interactions this model has the feature that the locally scaled breakpoint energy is only a weak function of slow dynamical effects. This is an important consequence of our model. It shows that dynamical effects do not impact the kinetic nature of the physics of E^* which we introduced in the second section of this paper. It is therefore not surprising that a relatively narrow histogram, of $E^*/(kT_c)$, such as obtained in Figure 4, could be obtained for a diverse collection of data in and out of evolving stream patterns.

The variation of plasma quantities, scaled with distance l/L along the compressed flux tube, centered at maximum compression, according to this model are shown in Figure 10 (l is the arc length along the local tube of force, and L the longitudinal scale length of the core compression). Panel A shows the total density enhancement and the thermal electron temperature variation with arc length relative to their locally unperturbed values. The core density variation of panel D determines three variations of the thermal temperature in panel A referring to the isothermal ($\gamma = 1$), $\gamma = 7/6$, and adiabatic ($\gamma = 5/3$) polytropic indices, respectively. The density and temperature profiles of panel A determine, via the generalized Ohm's law, the variation of an electron's potential energy along the tube of force under the three assumptions of the thermal polytropic indices. The extrathermals locally experience no resistance (collisions), and they will be attracted toward the compression and gain kinetic energy en route from the uncompressed local region of the flux tube. The core population does not have the mobility to overcome their shielding responsibilities of nearby ions. Only the extrathermals are clearly free to be attracted to the free charge within the compression.

In panel C we show the computed variation of $n_h(r)$ according to our model which entails evaluating (7) by using (8)–(11). The extrathermal response at maximum core compression of ~200% ranges from a 5% enhancement of the halo for near-isothermal core behavior ($\gamma = 1$, 7/6) to an 18% reduction for adiabatic core behavior ($\gamma = 1.45$ yields an approximately 5% reduction of the halo). In performing these calculations we have assumed that the halo had a constant temperature of 7×10^5°K and that the unperturbed core temperature was 1.16×10^5°K. It is important to reemphasize that the depicted variations are those an observer would report moving along the local tube of force through the compression.

Before discussing measurements of the halo variations through stream-stream interaction regions we should comment on the confusing and uncritical use in the literature of the word 'compression' for any density enhancement which precedes the high-speed flow immediately before the fast velocity increase observed in typical time records. (We do not

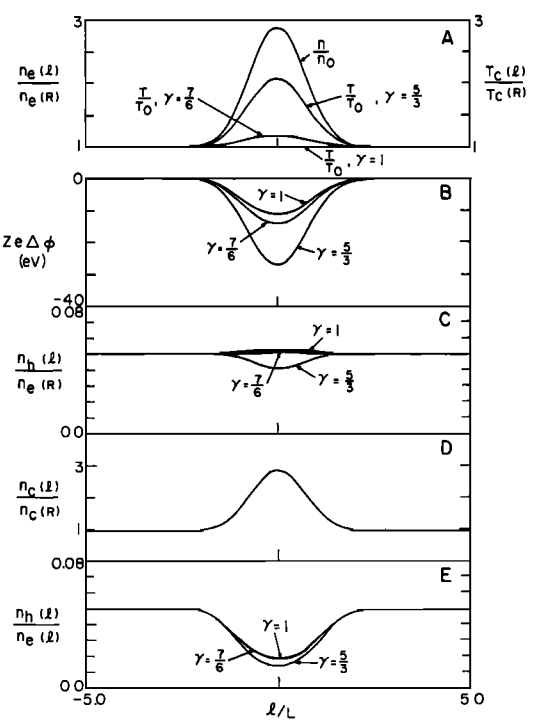

Fig. 10. Electron parameters through modeled compression region. Horizontal axis is arc length l along the tube of force divided by the scale L of the density compression of the core (see the text). Note that script els of the figure have been typeset in the text as lower case italic els.

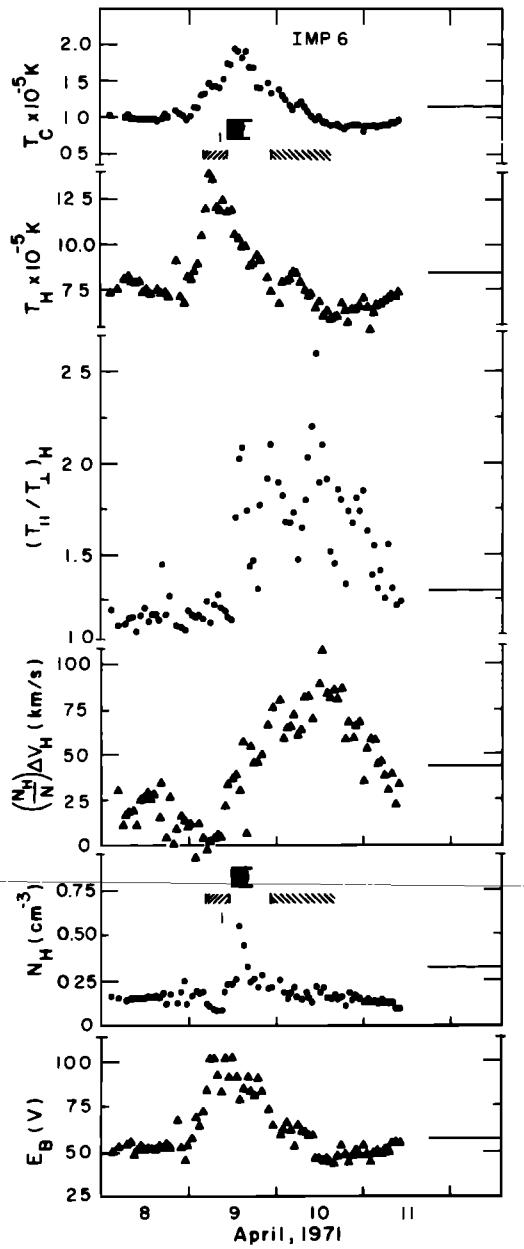

Fig. 11. Reproduced data figure from *Feldman et al.* [1975], showing electron variations in compression regions. The black bar has been added to indicate the present authors' opinion of where compression takes place (note that it takes place at a different location from that of the density maximum, which *Feldman et al.* [1975] term the compression).

mean the isolated noncompressive density enhancements structure in nearly uniform flow fields, discussed by *Gosling et al.* [1977].) A change in the number density, dn, may arise either from variations in size of a small volume element, $d(\Delta V)$; or changes in the number (ΔN) of particles in that volume:

$$dn = -\frac{\Delta N}{(\Delta V)^2} d(\Delta V) + \frac{d(\Delta N)}{\Delta V} \tag{12}$$

The variations with volume change are the compressive contributions to dn. The remaining contributions represent net change of number of particles in the volumes. As such, this latter contribution to density variations represents the boundary conditions on the reference volume (the halo density change computed above represents a combination of ΔV and ΔN). There is a growing body of evidence (experimental, e.g., *Rosenbauer et al.* [1977] and *Gosling et al.* [1977], and theoretical, e.g., V. J. Pizzo (private communication, 1978)) that a substantial portion of the density variation encountered prior to the steep stream velocity gradient is a remnant of the coronal boundary conditions in the initially denser, preceding slow stream which has been eroded by the dynamical consequences of filling in the rarefaction.

The compressive zones are therefore not necessarily at the maximum density before the rise in the stream profile. Given that proton heat conduction is almost negligible, it seems warranted to locate the compression zone (where tubes of force are constricted) by the detection of simultaneously enhanced proton temperatures centered on the rapidly increasing slope of the bulk speed profile.

Another intrinsic difficulty with examining temporal data records is that temporal variations do not translate into a unique picture of the spatial shapes of structures. This means, for example, that a density enhancement traversing the observer in 1 day at a fixed solar wind velocity U and imbedded magnetic field direction $\hat{B}$ implies relatively little about the spatial extent of the structure along the local tubes of force. The density enhancement could have almost any scale length along $\hat{B}$ when compared with the apparent transverse scale length as determined from the width of structures convected over the observer.

With these comments, we consider some published data from Imp 6 of the variations of the halo density through a stream interaction region reported by *Feldman et al.* [1975, Figure 12] and reproduced here as Figure 11. The subpanels from top to bottom indicate the temporal records of the core and halo temperatures, the halo-thermal anisotropy, the core 'drift' speed, the halo density, and the breakpoint energy E_B as defined in section 2 of this paper. The shaded zones denote, from left to right, 'the region of large density compression where the added line indicates the position of the density maximum, and the high velocity region beginning with the approximate position of the velocity maximum.' These authors draw the following conclusions about the halo density data (p. 4191): '5. The halo density does not share in the core density compression which precedes the high speed region. Instead it is observed to be enhanced immediately after the main proton compression region. In this sense the halo behaves more like an independent, ubiquitous collisionless electron gas which responds to stream interaction structures induced in the solar wind plasma (similar to the response of low energy solar protons to interplanetary disturbances).' We have indicated the zone of maximum compression on the basis of proton temperature T_p peak with a solid dark box above the halo density and core temperature traces. The halo density precipitously increases in the compression region that we have determined using T_p. This zone is also in a region of enhanced but not maximal total density and near the maximum electron core temperature. Also note that T_h is nearly a constant across this enhanced halo density region.

From our model results the density of the halo can be enhanced only for nearly isothermal compressions $\gamma \simeq 1$; $\gamma \simeq 7/6$ also yields a halo enhancement; $\gamma = 1.45$ yields a reduction. This behavior appears to be at variance with the core temperature enhancement with enhanced density of the temporal records of Figure 11 which can be translated into a cross-sectional cut of the three-dimensional variations at the stream interaction. However, as was discussed previously, the cross-sec-

tional profile of a variable across different tubes of force does not determine the corresponding profile along $\hat{B}$ without additional assumptions. A nearly isothermal core electron profile along flow tubes in the crest of the compression (black zone) is consistent with the temporal record and our model. If we pursue this line of reasoning, the heat transport along $\hat{B}$ from the compression away from the sun should be enhanced here in order to maintain nearly the same total electron temperature along the flux tube. This effect is not shown in this figure. However, this expected effect is clearly evident in Figure 8, where, centered on a different halo density enhancement in the compression zone (defined by the protons' black shading), there is an unusually large heat flow.

We thus conclude that the available data are consistent with the implications of our model of solar wind electrons even in the presence of slow variations. The steady state γ which we used to interpret the polarization potential and suggest the distant $T_c(r)$ profile also describes the slowly varying dynamic regime near compression regions. A portion of the T_c variation across adjacent flux tubes in the temporal records may therefore be interpreted as the remnants of coronal boundary conditions or the thermal history of the electrons en route to the point of observation as determined by the dynamics along those field lines which thread the compression pattern at some other radial distance.

In view of our conclusion that thermal electrons obey a polytrope law with index 7/6 it is appropriate to test our results by examining a recent report by *Feldman et al.* [1978*b*] that concludes that $\gamma \simeq 1.45$, which is more nearly adiabatic ($\gamma = 5/3$) than isothermal ($\gamma = 1$). Their analysis was performed on the data partially displayed in our Figure 8, where these authors concentrated their attention on the fast compressed gas. They considered the observed temporal variation of the data which at 1 AU is principally across local tubes of forces. A crucial assumption of their analysis is that the streamline constants at the footpoints of the sampled flux tubes have the same value on all sampled streamlines. The polytrope relation

$$P(l, s)/P_0(0, s) = [\rho(l, s)/\rho(0, s)]^{\gamma} \tag{13a}$$

where s indicates a given streamline, has been approximated as

$$P(l, s) = \Sigma_0[\rho(l, s)]^{\gamma} \quad \Sigma_0 = \text{const} \tag{13b}$$

where $l(s)$ denotes arc length along the streamline labeled s. The reported statistical analysis pertains to adjoining streamlines of compressed fast plasma, cf. Figure 12*a* near the leading edge of the stream. Their analysis derived the effective least square γ_{eff}, which 'characterizes' the data under the assumption that the variation of the streamline constant Σ may be ignored on adjacent tubes of the force which thread the compression region and have been sampled. This assumption was made on the grounds that electron parameters are observed at 1 AU to be very homogeneous in the uncompressed high-speed wind.

As the thermal electrons dominate the partial pressure and density, the electron gas may behave in lowest order as a polytropic gas whenever the approximations leading to (2) are fulfilled (probably $r > 20\ R_S$).

$$P_e(l, s) \propto \rho_e(s)^{\gamma_{\text{eff}}} \quad \gamma_{\text{eff}} = 1.45 \pm 0.05 \tag{14}$$

we now inquire what variation of streamline constant $\Sigma(s)$ is required to reconcile γ_{eff} with $\gamma_* = 7/6$. If

$$\Sigma(s) = P^*/(\rho^*)^{\gamma_*} \cdot \rho[l(s)]^{(\gamma_* - \gamma_{\text{eff}})} \tag{15a}$$

then these authors' γ_{eff} can be reconciled with the body of evidence compiled in this paper that $\gamma_* \simeq 7/6 \pm 0.06$. We thus determine that

$$\gamma_* - \gamma_{\text{eff}} = 7/6 - 1.45 \cong -0.28 \pm 0.08 \tag{15b}$$

Thus for $\rho[l(s)]$ varying by a factor of 5 as in these authors' work, Σ would have to have had a percentage variation of

$$\frac{d\Sigma}{\Sigma} \simeq \frac{\Sigma - \Sigma^*}{\Sigma^*} = 57 \pm 8\% \qquad \Sigma(s')s' > s^* \tag{16}$$

where Σ^* is determined at the maximum compression within high-speed flow (at s^* as indicated in Figure 12). Is it reasonable that Σ^* be smallest on the most compressed flow tube?

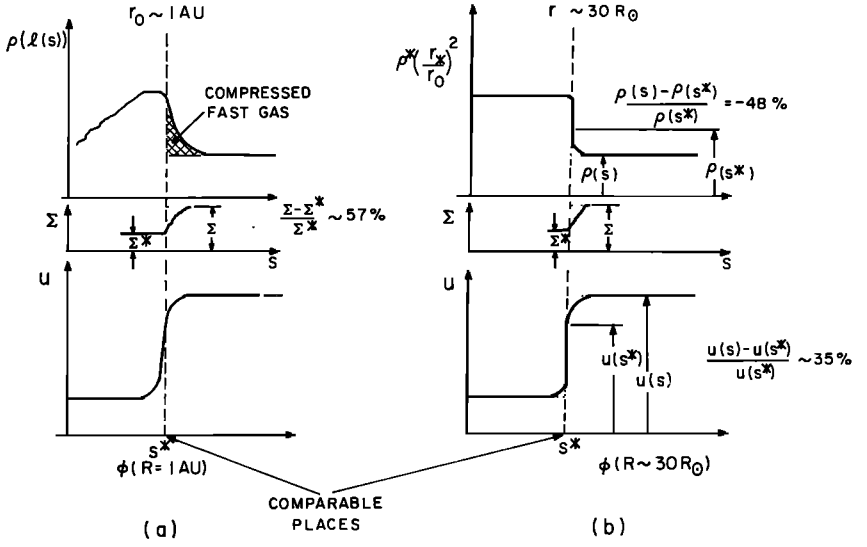

Fig. 12. (*a*) Schematic of density ρ, stream tube constant Σ, and speed u, across stream tubes observed at 1 AU. The horizontal axis is heliocentric longitude of the observer. (*b*) Hypothetical variations at $R = 30\ R_S$ which reconcile $\gamma_{\text{eff}} = 1.45$ with an actual $\gamma^* = 7/6$. The 'shoes' discussed in the text refer to the gradual transitions or ramps between flow states and are to be contrasted with the dotted square waves.

Since Σ is a stream tube constant over a radial range, it seems appropriate to answer this question at the innermost boundary ($R \sim 20$–$30\ R_S$) where we could defend by previous arguments that the same polytropic behavior obtains. The assumptions made by *Feldman et al.* [1978*b*] is that the stream tube constants at the inner boundary are uniform and that Σ is a constant from heliocentric longitude $\phi(s^*)$ into the high-speed wind ($s > s^*$) even though these initial conditions have been impressed by the wind in which electrons are not behaving as a polytropic gas of the same γ or may not be polytropic at all. There exists a body of evidence which tends to suggest that ρU^β = const at 1 AU ($\beta \sim 1.5$) [*Burlaga and Ogilvie,* 1970]; mesalike structures in flow velocity reported by *Rosenbauer et al.* [1977] at 0.3 AU show a similar anticorrelation of density ρ and solar wind speed U. These mesalike structures approximate, but are not, square waves; the corners of the speed profiles are rounded as schematized in Figure 12*b*. Assuming that ρU^β is a constant relation, it seems that the density profile will also have a complementary 'shoe' to the descent from dense slow flow to sparse, fast flow. If we assume that the electron pressure is a constant across stream tubes, then we can relate percentage changes in Σ to similar variations in speed as

$$\frac{d\Sigma}{\Sigma} = \beta\gamma_* \frac{dU}{U} \qquad s > s^*\ P(s, 30\ R_S) = P_0 \qquad (17)$$

For the discrepancy between γ_{eff} and γ_* to be attributed to flow tube constant variations, we require the density shoe to extend over such longitudes $\phi(s)$, $s > s^*$, from 63% of the mesa stream value until the speed profile reaches a flat maximum. This is a relatively thin and sharp speed stream. Under the alternate assumption that $T_e(s)$ is constant in longitude at 30 R_S, we require the density shoe to extend over the entire transition from low- to high-speed flow; this is a very broad 'stream-stream' boundary. The Helios data seem to indicate that high-speed streams at 60 radii are narrow rather than as broad as the isothermal assumption requires. We have indicated in Figure 12*b* the percentage variations we require in order that values of $\gamma_* = 7/6$ and γ_{eff} may be reconciled with $P(s, 30\ R_S) = P_0$. This is a plausible resolution of the interpretation of these data and our previous arguments in favor of $\gamma_* = 7/6$.

6. Discussion and Summary

From a detailed consideration of Coulomb collision dynamics and the inhomogeneity of the solar wind we have calculated the scaling of the transition kinetic energy E^* of the local electron distribution for $r > 0.45$ AU to be

$$E^* \simeq 7kT_c$$

We showed that this scaling is supported on average by all of the Mariner 10 data (independent of radius) between 0.45 and 0.9 AU and also by a statistical analysis of published Imp (1 AU) data. Electrons with kinetic energies greater than E^* are a special subpopulation of the suprathermal electrons that we have called the extrathermals. The extrathermals have been shown to be the same group previously named the halo or hot component.

By experimental and theoretical arguments we suggest that the transition energy $E^*(r)$ and the polarization potential energy $e\Phi(r)$ are on average synonymous in steady state for all radii greater than 0.45 AU where Hall effect and resistive contributions to Φ are not important. A necessary condition that this result can be true is that the core electrons obey a polytrope condition

$$P = \Sigma(s)\rho^\gamma \qquad \gamma \simeq 7/6 \pm 0.06$$

where $\Sigma(s)$ are (perhaps different) streamline constants. An ancillary priviso for the use of the suggested polytrope behavior of thermal electrons as part of a locally neutral magnetofluid–dynamic plasma description must also be understood: the scale length of the gradients of the component of the bulk velocity along the magnetic field should be long in comparison with the electron mean free path λ_{mfp}.

When the density variation becomes inverse square with radius this polytrope law suggests that

$$T_c = Ar^{-\alpha} \qquad \alpha = 1/3$$

which is consistent with recent in situ determinations on Mariner 10 (0.45–0.9 AU) [*Ogilvie and Scudder,* 1978], Vela [*Montgomery et al.,* 1968], and Voyager 2 (1.25–2.3 AU) [*Sittler et al.,* 1978] of $\alpha = 0.3 \pm 0.08$, $0.21 < \alpha < 0.4$, and $\alpha = 0.34 \pm 0.16$, respectively. This asymptotic radial exponent of electron temperature variation is greater than but very nearly 2/7, as suggested by the fluid solution of *Noble and Scarf* [1963] and *Parker* [1964], and less than the *Whang and Chang* [1965] solution, which has an exponent of 2/5. This asymptotic variation also implies that the mean free path for Coulomb scattering divided by the scale height along B, $K_\parallel$ will become increasingly smaller and thus electrons in the ecliptic will become more fluidlike with increasing radial distance. If the same radial variations obtain for density and temperature over the solar poles, then $K_\parallel$ grows with radius as $r^{+1/3}$, indicating increasing departures from a Coulomb collisionally isotropized core and fluid behavior as r increases over the pole.

It is by no means clear, even now, whether the suggested equivalence of $E^*(r)$ with $e\Phi(r)$ is a general result for a plasma with $T_e \gg (m_e/m_p)T_p$ and an open magnetic topology when resistive and Hall effects are negligible. We have shown that this condition implies a localized (polytrope) description for the thermal electrons which provide the majority of the shielding neutralizing charge density for the ions. In this sense this steady state condition is nearly the requirement that a system of sufficient scale given sufficient time (steady state ($t \rightarrow \infty$)) will adjust itself, so that the free charge is minimal. This association seems a posteriori reasonable in steady state, since electrons with kinetic energy $E > E^*$ are energetically unbound everywhere in the system and are correspondingly also allowed by Coulomb properties to respond to thermodynamic forces by being energetically free with ballistic ranges against pitch angle changes long compared to the local mean free path. These particles, however, may be dynamically quasi-trapped via the cumulative backscattering they experience provided the system is large enough. The heliosphere appears to be large enough. This kinetic (local) and electrostatic potential (global) compatibility may be of more general importance than its application to the current problem.

We have also shown theoretically that E^*/kT_c is nearly independent of the slow dynamical evolution at stream boundaries. This feature of our model is an important consistency check of the fundamentally kinetic nature of the meaning of E^* as derived solely from the properties of the Coulomb cross section. Had it been otherwise, we would have the unacceptable circumstance that the large-scale dynamics of the solar wind affects local kinetic properties of the plasma. (Recall that E^* was defined in section 2 as the energy below which escape from the local proximity was less than 3σ possibility.)

A straightforward calculation with this model for conditions within a stream compression region near 1 AU shows that the extrathermal (halo) density can either increase or decrease within compression regions depending on the nature of the effective polytropic gamma of the local core compression. This sensitivity to the local nature of the core compression results from the interaction of the modified polarization electric field (determined primarily by the gradients of core T_c, n_c) with extrathermal electrons which are passing along the compressed tubes of force. In this sense the halo and core populations are locally coupled (even in slowly evolving stream interaction regions) through the strong force of the polarization potential.

We concluded that for two published examples of n_{halo} variation at stream boundaries the halo density probably does increase within stream interaction regions, contrary to the conclusions of *Feldman et al.* [1975]. This conclusion is supported by our model calculations, which predict halo enhancements when the core compression is more nearly isothermal (e.g., 7/6) than adiabatic (e.g., 1.45)—together with the corollary that to maintain a nearly isothermal compression very large heat fluxes should be observed parallel to B within the compression region. This latter correlation is observed in the same paper. We have also suggested a way to reconcile their value with $\gamma = 7/6$ by modest streamline constant variations. There is thus no contradiction to the idea that the thermal electrons compress as if they were nearly isothermal ($\gamma = 7/6$) at stream-stream interaction boundaries.

In this paper we have presented strong observational support from data obtained on three different satellites reported by three independent experimental groups for all of the theoretically predicted correlations of paper 1, namely, the following:

1. Subthermal ($E < kT_c$) electrons behave most nearly as a classical gas—such a gas compressively heats and expansively cools to the extent that heat transport permits and will participate in stream-induced enhancements of the ions because of their strong collisional coupling to the ions and electrostatic plasma shielding requirements.

2. The solar wind extrathermal fraction of the electron density is anticorrelated within steady state stream patterns with the local bulk speed (if it is nearly the asymptotic value).

3. The extrathermal electrons (with energy $E > 7\ kT_c$) do form a spectrally distinguishable subpopulation. The differential 'temperature' of these particles is observed to be anticorrelated with the local bulk speed.

4. The heat flux carried by electrons is anticorrelated with the bulk speed.

5. The extrathermal 'temperature' is nearly independent of radius in the inner heliosphere.

We thus conclude that the global and local Coulomb collisional effects discussed in paper 1 and elaborated here are essential aspects of the solar wind plasma as it is observed. The experimental support which the predictions of the theory in paper 1 enjoy strongly suggests that the further development of that theory is warranted with the ultimate objective of understanding the impact that global heat transport has on the physics of coronal expansions.

Acknowledgments. One of us (J.S.) would like to acknowledge discussions with and manuscript comments from L. F. Burlaga, A. J. Klimas, K. W. Ogilvie, and V. J. Pizzo of Goddard Space Flight Center (GSFC) and H. S. Bridge of the Massachusetts Institute of Technology (MIT). A portion of this research (for S.O.) was supported by NASA grant NGL-22-009-015. We also acknowledge the work of the team headed by H. S. Bridge, Principal Investigator, which designed the Mariner 10 Plasma Science Experiment at GSFC, MIT, the Jet Propulsion Laboratory, Los Alamos and Scientific Laboratory (LASL). In addition, we would like to acknowledge the data support effort made by Earl Tech of LASL and Steve Curtis, Steve Carchedi, and Len Moriarty of GSFC.

The Editor thanks A. J. Hundhausen and another referee for their assistance in evaluating this paper.

REFERENCES

Braginskii, S. I., Transport processes in a plasma, in *Reviews of Plasma Physics,* vol. I, Consultants Bureau, New York, 1965.

Burlaga, L. F., and K. W. Ogilvie, Magnetic and thermal pressures in the solar wind, *Solar Phys., 15,* 61, 1970.

Burlaga, L. F., K. W. Ogilvie, D. H. Fairfield, M. D. Montgomery, and S. J. Bame, Energy transfer at colliding streams in the solar wind, *Astrophys. J., 164,* 137, 1971.

Feldman, W. C., J. R. Asbridge, S. J. Bame, M. D. Montgomery, and S. P. Gary, Solar wind electrons, *J. Geophys. Res., 80,* 31, 1975.

Feldman, W. C., J. R. Asbridge, S. J. Bame, and J. T. Gosling, High-speed solar wind flow parameters at 1 AU, *J. Geophys. Res., 81,* 28, 5054, 1976.

Feldman, W. C., J. R. Asbridge, S. J. Bame, J. T. Gosling, and D. S. Lemons, Characteristic electron variations across simple high-speed solar wind streams, *J. Geophys. Res., 83,* 5285, 1978*a*.

Feldman, W. C., J. R. Asbridge, S. J. Bame, J. T. Gosling, and D. S. Lemons, Electron heating within interaction zones of simple solar wind high-speed streams, *J. Geophys. Res., 83,* 5297, 1978*b*.

Goldstein, B. E., and J. R. Jokipii, Effects of stream-associated fluctuations upon the radial variation of average solar wind parameters, *J. Geophys. Res., 82,* 1095, 1977.

Gosling, J. T., E. Hildner, J. R. Asbridge, S. J. Bame, and W. C. Feldman, Noncompressive density enhancements in the solar wind, *J. Geophys. Res., 82,* 22, 1977.

Hundhausen, A. J., Solar wind stream interactions and interplanetary heat conduction, *J. Geophys. Res., 78,* 7996, 1973.

Hundhausen, A. J., and M. D. Montgomery, Heat conduction and nonsteady phenomenon in the solar wind, *J. Geophys. Res.,* 76, 2236, 1971.

Jockers, K., Solar wind models based on exospheric theory, *Astron. Astrophys. 6,* 219, 1970.

Maxson, C. W., and G. S. Vaiana, Determination of plasma parameters from soft X-ray images for coronal holes (open magnetic configurations) and coronal large scale structures (extended closed field configurations), *Astrophys. J., 215,* 919, 1977.

Montgomery, M. D., S. J. Bame, and A. J. Hundhausen, Solar wind electrons, Vela 4 measurements, *J. Geophys. Res., 73,* 4999, 1968.

Munro, R. H., and B. V. Jackson, Physical properties of a polar coronal hole from 2–5 R, *Astrophys. J., 213,* 874, 1977.

Neubauer, F., G. Musmann, and G. Dehmel, Fast magnetic fluctuations in the solar wind: Helios 1, *J. Geophys. Res., 82,* 22, 1977.

Noble, L. M., and F. L. Scarf, Conductive heating of the solar wind, I, *Astrophys. J., 138,* 1169, 1963.

Ogilvie, K. W., and J. D. Scudder, The radial gradients and collisional properties of solar wind electrons, *J. Geophys. Res., 83,* 3776, 1978.

Parker, E. N., *Interplanetary Dynamical Processes,* John Wiley Interscience, New York, 1963.

Parker, E. N., Dynamical properties of stellar coronas and stellar winds, II, Integration of the heat flow equation, *Astrophys. J., 139,* 93, 1964.

Perkins, F., Heat conductivity, plasma instabilities, and radio star scintillations in the solar wind, *Astrophys. J., 179,* 637, 1973.

Rawls, J. W., M. S. Chu, and F. L. Hinton, Transport properties of a toroidal plasma of intermediate to high collision frequencies, *Phys. Fluids, 18,* 9, 1160, 1975.

Rosenbauer, H., R. Schwenn, E. Marsch, B. Meyer, H. Miggenreider, M. D. Montgomery, K. H. Mulhauser, W. Pilipp, W. Voges, and S. M. Zink, A survey of initial results of the Helios plasma experiment, *J. Geophys., 42,* 561, 1977.

Rossi, B., and S. Olbert, *Introduction to the Physics of Space,* McGraw-Hill, New York, 1970.

Schultz, M., and A. Eviatar, Electron-temperature asymmetry and the structure of the solar wind, *Cosmic Electrodynamics, 2,* 402, 1972.

Scudder, J. D., and S. Olbert, Local and global processes which Im-

pact solar wind electrons, in *Solar Wind Four,* edited by H. Rosenbauer, in press, Springer, New York, 1978.

Scudder, J. D., and S. Olbert, A theory of local and global processes which affect solar wind electrons, 1, The origin of typical 1-AU velocity distribution functions—Steady state theory, *J. Geophys. Res., 84,* 2755, 1979.

Serbu, G. D., Explorer 35 observations of solar wind electron density, temperature, and anisotropy, *J. Geophys. Res., 77,* 1703, 1972.

Sittler, E. C., Jr., and S. Olbert, Radial profiles of the solar wind velocity, temperature, and heat flux vector based on the empirical density profile and empirical magnetic field line topology (abstract), *Eos Trans. AGU, 58*(6), 484, 1977.

Sittler, E. C., Jr., J. D. Scudder, and J. Jessen, Radial variation of solar wind thermal electrons between 1.36 and 2.25 AU: Voyager 2, in *Solar Wind Four,* edited by H. Rosenbauer, in press, Springer, New York, 1978.

Spitzer, L., Jr., *Physics of Fully Ionized Gases,* John Wiley Interscience, New York, 1962.

Whang, Y. C., and C. C. Chang, An inviscid model of the solar wind, *J. Geophys. Res., 70,* 4175, 1965.

(Received January 30, 1979;
revised June 12, 1979;
accepted June 28, 1979.)